THE JOURNAL OF BIOLOGICAL CHEMISTRY VOL. 285, NO. 51, pp. 40351–40361, December 17, 2010

Structural Basis for Hormone Recognition by the Human CRFR2α G Protein-coupled Receptor*[S]

Received for publication, September 16, 2010, and in revised form, October 10, 2010 Published, JBC Papers in Press, October 21, 2010, DOI 10.1074/jbc.M110.186072

Kuntal Pal[‡§], **Kunchithapadam Swaminathan**[§1], **H. Eric Xu**[‡2], **and Augen A. Pioszak**[‡3]

From the [‡]*Laboratory of Structural Sciences, Van Andel Research Institute, Grand Rapids, Michigan 49503 and the* [§]*Department of Biological Sciences, National University of Singapore, Singapore 117543*

The mammalian corticotropin releasing factor (CRF)/urocortin (Ucn) peptide hormones include four structurally similar peptides, CRF, Ucn1, Ucn2, and Ucn3, that regulate stress responses, metabolism, and cardiovascular function by activating either of two related class B G protein-coupled receptors, CRFR1 and CRFR2. CRF and Ucn1 activate both receptors, whereas Ucn2 and Ucn3 are CRFR2-selective. The molecular basis for selectivity is unclear. Here, we show that the purified N-terminal extracellular domains (ECDs) of human CRFR1 and the CRFR2α isoform are sufficient to discriminate the peptides, and we present three crystal structures of the CRFR2α ECD bound to each of the Ucn peptides. The CRFR2α ECD forms the same fold observed for the CRFR1 and mouse CRFR2β ECDs but contains a unique N-terminal α-helix formed by its pseudo signal peptide. The CRFR2α ECD peptide-binding site architecture is similar to that of CRFR1, and binding of the α-helical Ucn peptides closely resembles CRF binding to CRFR1. Comparing the electrostatic surface potentials of the ECDs suggests a charge compatibility mechanism for ligand discrimination involving a single amino acid difference in the receptors (CRFR1 Glu104/CRFR2α Pro-100) at a site proximate to peptide residue 35 (Arg in CRF/Ucn1, Ala in Ucn2/3). CRFR1 Glu-104 acts as a selectivity filter preventing Ucn2/3 binding because the nonpolar Ala-35 is incompatible with the negatively charged Glu-104. The structures explain the mechanisms of ligand recognition and discrimination and provide a molecular template for the rational design of therapeutic agents selectively targeting these receptors.

The corticotropin releasing factor (CRF)[4]/urocortin (Ucn) family of peptides comprises four members in mammals including CRF, Ucn1, Ucn2, and Ucn3 that exert their actions through either of two cell surface G protein-coupled receptors (GPCRs), CRFR1 and CRFR2 (1–3). Distinct genes encode the four peptides and two receptors (4–9). The peptides form α-helices that are structurally very similar (10), but they exhibit unique pharmacological profiles. CRF activates both receptors but is more potent at CRFR1. Ucn1 exhibits equal potency for both receptors, whereas Ucn2 and Ucn3 are selective for CRFR2. CRFR1 is highly expressed in the CNS and is also present in peripheral tissues. CRFR2 is expressed in the CNS and peripheral tissues including the heart, vasculature, skeletal muscle, and gastrointestinal tract. CRF plays a central role in coordinating endocrine, autonomic, and behavioral responses to stress via activation of CRFR1 in the brain. The Ucn peptides exert actions in central and peripheral tissues where they modulate cardiovascular, immune, gastrointestinal, and reproductive functions in response to stress (11). The CRFR2-selective Ucn2 and -3 have recently emerged as important metabolic regulators that link stress and energy homeostasis (12–15). Urocortins can also affect tumor biology as a consequence of the CRFR2 role as a suppressor of vascularization (16). Exogenously administered Ucn1 or Ucn2 inhibited tumor growth in mice (17, 18). The involvement of CRF/Ucn family peptides and their receptors in diverse pathophysiological states has generated intense interest in developing therapeutic agents that selectively target the receptors. CRFR1-selective antagonists have the potential to treat anxiety, depression, and related disorders (19), and CRFR2-selective agonists have the potential to treat heart failure (20), hypertension (21), and other disorders.

The CRF receptors belong to the class B/secretin family GPCRs that includes the receptors for parathyroid hormone (PTH), calcitonin, glucagon, glucagon-like peptide 1 (GLP1), and several other clinically important peptides (22). The receptors have a bipartite domain structure consisting of an N-terminal extracellular domain (ECD) of about 100–150 amino acids linked to a 7-transmembrane helical bundle domain embedded in the plasma membrane. Peptide binding spans the two domains, with the C-terminal portion of the peptide binding to the ECD to impart high affinity and the N-terminal portion binding to the 7-transmembrane domain to activate the receptor. CRF/Ucn family peptides are 38–41

* This work was supported, in whole or in part, by National Institutes of Health Grant GM087413 (to H. E. X. and A. A. P.). This work was also supported in part by the Jay and Betty Van Andel Foundation (to H. E. X., A. A. P., and K. P.), grants from the Ministry of Education, Singapore, and Biomedical Research Council (to K. S.), and a Research Scholarship from the National University of Singapore (to K. P.).

[S] The on-line version of this article (available at http://www.jbc.org) contains supplemental Table S1 and Fig. S1.

The atomic coordinates and structure factors (codes 3N96, 3N95, and 3N93) have been deposited in the Protein Data Bank, Research Collaboratory for Structural Bioinformatics, Rutgers University, New Brunswick, NJ (http://www.rcsb.org/).

[1] To whom correspondence may be addressed. E-mail: dbsks@nus.edu.sg.
[2] To whom correspondence may be addressed. E-mail: eric.xu@vai.org.
[3] Present address and to whom correspondence may be addressed: Dept. of Biochemistry and Molecular Biology, University of Oklahoma Health Sciences Center, Oklahoma City, OK 73104. E-mail: augen-pioszak@ouhsc.edu.

[4] The abbreviations used are: CRF, corticotropin releasing factor; mCRFR2β, mouse CRFR2β; hCRFR2β, human CRFR2β; CRFR, CRF receptor; Ucn, urocortin; ECD, extracellular domain; PTH, parathyroid hormone; PTH1R, PTH receptor; GLP1, glucagon-like peptide 1; ADA, [(carbamoylmethyl)imino]diacetic acid; ASU, asymmetric unit; MBP, maltose-binding protein; GPCR, G protein-coupled receptor.

amino acids in length and have a C-terminal amide group that is strictly required for bioactivity. The 26–41 fragments constitute the minimal ECD binding region (23, 24). Both the ECD and the 7-transmembrane domains of the CRF receptors contribute to selectivity (25–28), but the structural basis for peptide discrimination is unclear.

CRFR1 and CRFR2 exhibit 68% amino acid sequence identity, with the most divergence occurring in the ECDs. CRFR1 exists as a single functional isoform, although several nonfunctional isoforms have been identified (29). CRFR2 has three functional full-length isoforms, α, β, and γ, that differ only at the extreme N terminus of the receptor (3). In humans, the CRFR2β isoform is expressed in the brain, and the CRFR2α isoform predominates in the periphery. CRFR1 and CRFR2β are produced with an N-terminal signal peptide that is cleaved in the endoplasmic reticulum to yield the mature receptor (26, 27). In contrast, the CRFR2α isoform contains a unique pseudo signal peptide that is not removed from the mature receptor (30). The function and structural feature of the pseudo signal peptide is an open question.

Recent structural advances have begun to elucidate the mechanisms of ligand recognition by the CRF receptors. There are two NMR structures, including the mouse CRFR2β ECD in complex with the non-selective CRF-like antagonist astressin (23) and the human CRFR1 ECD in complex with a high affinity CRF-like agonist (31). There are also three crystal structures of the human CRFR1 ECD, one in a ligand-free form and two in distinct CRF-bound states (24). These structures reveal the architecture of the ECD fold for hormone binding and the conformational changes induced by such binding. The ECD forms a short consensus repeat fold that consists of two β-sheets each with two anti-parallel β-strands held together by three conserved disulfide bonds. The CRFR1 ECD-CRF crystal structure clearly elucidated the mechanism of endogenous ligand binding. CRF-(26–41) forms a continuous α-helix that occupies a shallow groove in the receptor surface formed at the interface of three loop regions. The bimolecular interaction is anchored at the peptide C terminus by a network of hydrogen bonds involving the amide group and the docking of the Met-38 side chain into a hydrophobic pocket on the receptor surface. Interestingly, the location of the peptide-binding site on the surface of the CRFR1 ECD differs significantly from that of other class B GPCRs (24). The structural advances expanded our understanding of ligand binding, but the structural basis for recognition and discrimination of the Ucn peptides remains unclear. In addition, the functions of the distinct N-terminal regions of the three CRFR2 isoforms and the structural features of the α isoform pseudo signal peptide are unknown.

Here we demonstrate that the purified ECDs of hCRFR1 and the α isoform of hCRFR2 are sufficient to discriminate CRF/Ucn family peptides, and we present three crystal structures of the CRFR2α ECD in complex with Ucn1, -2, or -3. The structures indicate that the pseudo signal peptide of CRFR2α forms an N-terminal α-helix that is similar to those present in other class B GPCRs, such as the receptors for PTH and GLP1, but absent in mCRFR2β. Comparison of the structures with the hCRFR1 ECD-CRF complex reveals the mechanism of ligand selectivity to involve an electrostatic charge compatibility mechanism that is facilitated by a single amino acid difference in the CRFR1 and CRFR2 ECDs. The structures provide the first views of a CRFR2 ECD-Ucn peptide complex and will aid in the rational design of therapeutic agents selectively targeting these receptors.

EXPERIMENTAL PROCEDURES

Molecular Cloning—Gene fragments encoding residues 1–117 or 3–104 of the α isoform of the human CRFR2 receptor were PCR-amplified from a cDNA clone obtained from the Missouri S&T cDNA resource center. The resulting fragments were digested with EcoRI and NotI restriction endonucleases and inserted into the previously described pETDuet1/MBP/DsbC vector (32) to encode a fusion protein consisting of bacterial maltose-binding protein (MBP) followed by the linker amino acid sequence NAAAEF and residues 1–117 or 3–104 of CRFR2. The constructs also contain a C-terminal His_6 tag. The 1–117 construct was used for functional studies, and the 3–104 construct was used for crystallization.

Protein Purification and Peptide Synthesis—The MBP-CRFR1 ECD-His_6 fusion protein, containing residues 24–119 of human CRFR1 fused to the C terminus of MBP, was previously described (24). The MBP-CRFR2α-ECD-His_6 proteins (1–117 or 3–104) were expressed in the *Escherichia coli* strain Origami B (DE3) (Novagen) with induction by isopropyl 1-thio-β-D-galactopyranoside (0.2 mM) at 16 °C overnight. The purification process was similar to that previously described for MBP-CRFR1 ECD (24) except that pH 8.0 buffers were used. In brief, cells were broken using a homogenizer at 10,000 p.s.i., and the protein was purified using nickel-chelating-Sepharose (GE Healthcare) and amylose columns (New England Biolabs), making use of the His_6 and MBP tags, respectively. Disulfide shuffling *in vitro* was carried out in a redox buffer of 1 mM reduced glutathione and 1 mM oxidized glutathione overnight at 20 °C. Superdex 200 gel filtration chromatography (GE Healthcare) was used to separate the properly folded, monomeric protein from aggregated material. A final ion-exchange step using a 1-ml HiTrap Q column (GE Healthcare) yielded a highly purified sample. Peptides were custom synthesized and HPLC-purified by New England Peptide or Peptide 2.0. All peptides contained an additional tyrosine residue at their N terminus to permit quantitation by UV absorbance at 280 nm and a C-terminal amide group unless otherwise noted.

Crystallization, Data Collection, Structure Solution, and Refinement—The MBP-CRFR2α-ECD protein was dialyzed to 10 mM Tris-HCl (pH 8.0), 50 mM NaCl, 1 mM maltose, 1 mM EDTA at 4 °C overnight. Protein:peptide complexes were formed by mixing them at a 1:1.2 molar ratio and incubating for 6 h. The Ucn1-, Ucn2-, and Ucn3-complexed samples were spin-concentrated to 22.5, 18.2, and 14.8 mg/ml, respectively, and directly used for crystallization. The Ucn1-complexed crystals were grown in an optimized condition of 10% PEG 6000, 0.1 M sodium acetate (pH 4.6), 0.1 M $MgCl_2$, and 14% glycerol using the hanging drop vapor diffusion method. The Ucn2-complexed crystals were obtained in 0.1 M ADA

(pH 6.0), 8% PEG 6000, 0.1 M $MgCl_2$, and 12% glycerol, and the Ucn3-complexed crystals were grown in 9% PEG4000, 0.1 M sodium acetate (pH 4.6), and 16% glycerol. All three crystal forms were cryoprotected by raising the glycerol concentration to 25%. The crystals were flash-frozen by immersion in liquid N_2.

Diffraction data were collected from single crystals at LS-CAT beamlines 21-ID-F and 21-ID-D (Advanced Photon Source), and the data were processed with HKL2000 (33). The structures were solved by molecular replacement using the PHASER program (34) in the CCP4 suite (35). COOT (36) was used for model rebuilding, and REFMAC5 (37) was used for refinement. The molecular replacement solution for the Ucn3-bound structure was obtained using two separate search models corresponding to MBP and the ECD from the human parathyroid hormone receptor (PTH1R) from PDB coordinate file 3H3G (38). The refined CRFR2α ECD model was then used as the ECD molecular replacement search model for the Ucn1- and Ucn2-bound structures. NCS restraints were used in all refinements as well as TLS refinement in the final stages. The data collection and refinement statistics are summarized in Table 1. Structure figures were prepared with PyMol (39). Electrostatic surface potential calculations were performed with APBS (40).

AlphaScreen Luminescent Proximity Assay for Peptide-Receptor Interaction—The interaction between peptides and the MBP-CRFR1-ECD-His_6 or MBP-CRFR2α-ECD-His_6 proteins was analyzed using AlphaScreen technology (PerkinElmer Life Sciences) essentially as previously described (38). MBP receptor ECD-His_6 protein (75 nM) was incubated with N-terminal-biotinylated CRF-(12–41)NH_2 (50 nM) in the presence of increasing concentrations of unlabeled competitor peptides in a buffer of 50 mM MOPS (pH 7.4), 150 mM NaCl, 7 mg/ml fatty acid free BSA, and 5 μg/ml each of streptavidin-coated donor beads and nickel-chelate-coated acceptor beads. The reactions were incubated at 22 °C for 5 h to reach equilibrium, and the signal was recorded in 384-well microplates using an Envision 2104 plate reader (PerkinElmer Life Sciences). Nonlinear regression, as implemented in Prism 5.0 (GraphPad Software), was used to fit the data to a variable slope dose-response inhibition equation for determination of IC_{50} values. Control experiments to ensure that signal inhibition by competitor peptides was specific were carried out using a biotin-Gly_6-His_6 peptide (50 nM) in place of the MBP receptor and biotin-CRF to bring the donor and acceptor beads into proximity. In all cases the competitor peptides did not significantly diminish this control signal at the concentrations used in our experiments.

RESULTS

The N-terminal Extracellular Domains of CRFR1 and CRFR2α Are Sufficient to Determine the CRF/Ucn Family Peptide Selectivity Profiles Observed for the Full-length Receptors—To facilitate structural and functional analyses of CRF/Ucn family peptide binding to the CRFR2 receptor and to allow comparison with the CRFR1 receptor, we expressed and purified the N-terminal, ECD of the α isoform of human CRFR2 using the methodology we developed for purification of class B GPCR ECDs and previously applied to CRFR1 (24) and PTH1R (32, 38, 41). The CRFR2α ECD, consisting of residues 1–117 and containing the pseudo signal peptide sequence, was expressed in *E. coli* as a soluble fusion protein with MBP at its N terminus and a His_6 tag at its C terminus. Properly folded, monomeric fusion protein was obtained after *in vitro* disulfide shuffling in a redox buffer and purification by size exclusion and ion exchange chromatography. The purified sample migrated as a single, distinct band on non-denaturing (native) gel electrophoresis (supplemental Fig. 1).

The ability of the purified MBP-CRFR2α ECD-His_6 fusion protein and the previously described MBP-CRFR1 ECD-His_6 fusion protein (24) to bind CRF/Ucn family peptides was assessed using an AlphaScreen luminescent proximity assay (PerkinElmer Life Sciences). In this assay, N-terminal-biotinylated CRF-(12–41) attached to streptavidin-coated donor beads interacts with the MBP- ECD-His_6 fusion protein attached to nickel-chelate-coated acceptor beads to bring the two beads into proximity and generate a luminescent signal. Competition with unlabeled peptides can be used to estimate their binding affinity (38). CRF-(26–41) and Ucn1, -2, and -3 peptides corresponding to the 26–41 fragment of CRF (Fig. 1*A*) were used as competitors because previous studies indicated that this region was sufficient for ECD binding (23, 24). The CRFR1 ECD bound Ucn1 with an IC_{50} value in the 500 nM to 1 μM range and CRF with an ~10-fold lower affinity and did not exhibit detectable binding to Ucn2 nor Ucn3 (Fig. 1*B*). The CRFR2α ECD also bound Ucn1 with an IC_{50} value in the 500 nM to 1 μM range, but CRF binding was ~30-fold weaker, and Ucn2 and -3 exhibited detectable binding with IC_{50} values similar to CRF (Fig. 1*C*). These results indicate that the CRFR2α ECD purified in this study is functional and that the isolated ECDs of CRFR1 and CRFR2α are sufficient to determine the ligand selectivity profiles that are observed for the full-length receptors in their natural membrane environment.

The results reported here for the CRFR1 ECD differ from our previous study where we observed competition of the AlphaScreen signal by micromolar concentrations of Ucn2 and -3, suggesting their binding to the CRFR1 ECD (24). However, in subsequent experiments we discovered that an insufficient BSA concentration (0.1 mg/ml) in the reaction buffer permitted nonspecific inhibition of the signal to occur at high competitor peptide concentrations.[5] In the experiments reported here, we included a high BSA concentration (7 mg/ml) in the reactions, which prevented nonspecific inhibition of the signal as determined by control experiments carried out as described under "Experimental Procedures."

Crystallization and Structure Determination of the CRFR2α ECD in Complex with Ucn Peptides—We sought to determine crystal structures of the CRFR2α ECD in complex with the Ucn peptides to elucidate the structural bases for their recognition and discrimination by CRFR2α. Complexes of the MBP-CRFR2α ECD-His_6 fusion protein bound to synthetic fragments of Ucn1, -2, or -3 corresponding to residues 26–41

[5] A. A. Pioszak and H. E. Xu, unpublished data.

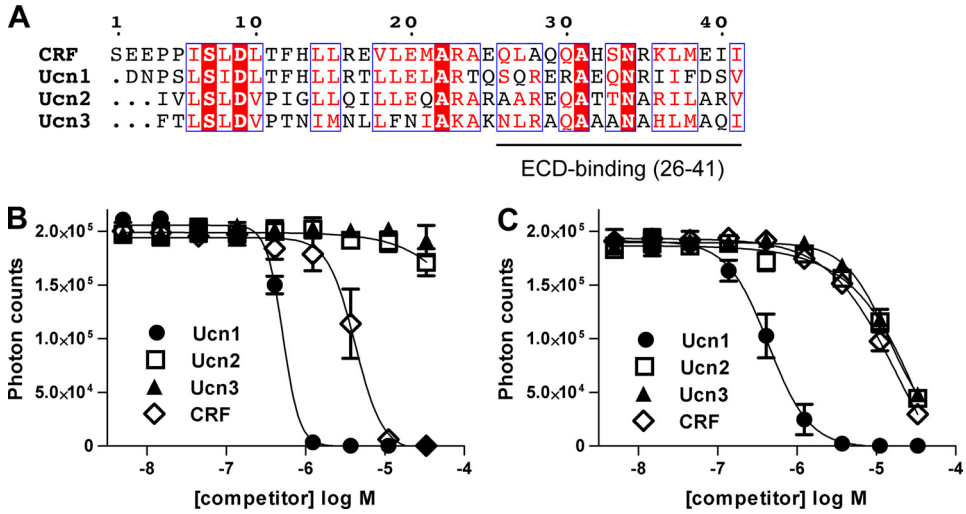

FIGURE 1. **Binding of CRF/urocortin family peptides to the purified CRFR1 and CRFR2α extracellular domains.** *A*, amino acid sequence alignment of the human CRF/Ucn family peptides is shown. *B* and *C*, competition curves show the ability of CRF-(26–41) and the equivalent fragments of Ucn1, -2, and -3 to inhibit the association of biotin-CRF-(12–41) and the MBP-CRFR1-(24–119)-His_6 (*B*) or MBP-CRFR2α-(1–117)-His_6 (*C*) fusion proteins in the AlphaScreen assay. The data represent the average of duplicate samples.

TABLE 1
Data collection and refinement statistics
r.m.s., root mean square.

	MBP-CRFR2α-ECD-Ucn1	MBP-CRFR2α-ECD-Ucn2	MBP-CRFR2α-ECD-Ucn3
Data collection			
Beamline	APS 21-ID-F	APS 21-ID-D	APS 21-ID-F
Space group	$P2_1$	$P2_1$	$C222_1$
a, b, c (Å)	54.06, 211.55, 107.83	54.31, 212.07, 107.32	54.28, 208.51, 212.55
α,β,γ (°)	90.00, 104.37, 90.00	90.00, 104.54, 90.00	90.00, 90.00, 90.00
Resolution range (Å)	50–2.75 (2.85–2.75)	50–2.72 (2.82–2.72)	50–2.50 (2.54–2.50)
Wavelength (Å)	1.0782	0.9787	0.9787
No. of observations	283,038	423,026	364,863
Unique reflections	59,140	62,181	42,571
Completeness (%)	95.5 (97.8)	99.2 (99.1)	99.1 (89.5)
Redundancy	4.8 (5.3)	6.8 (6.4)	8.6 (3.4)
I/σ	12.6 (2.1)	14.28 (2.82)	19.64 (2.30)
R_{merge} (%)	14.1 (69.9)	15.0 (70.9)	12.5 (47.6)
Refinement			
Resolution range	50–2.75	50–2.72	50–2.49
No. of reflections (total/test)	55,085/2,922	58,923/3,148	40,366/2,134
R_{cryst}/R_{Free} (%)	23.91/27.33	22.85/26.83	22.76/27.71
MBP-ECD mol/ASU	4	4	2
Mean B value (Å^2)	62.5	47.9	33.8
No. of TLS groups	12	10	5
No. of protein atoms	15050	14720	7371
No. of water atoms	104	272	124
No. of heterogen atoms	92 (4 maltose)	92 (4 maltose)	52 (2 maltose + 1 glycerol)
r.m.s. bond length deviation (Å)	0.015	0.010	0.010
r.m.s. bond angle deviation (°)	1.5	1.2	1.2
Ramachandran plot, %			
Most favored	91.2	93.7	93.2
Allowed	8.7	6.3	6.8
Generously allowed	0.2	0.0	0.0
Disallowed	0.0	0.0	0.0

were prepared and subjected to crystallization screening. Initial trials with the fusion protein containing residues 1–117 failed to yield any crystals, but shortening the N and C termini of the ECD to include only residues 3–104 yielded a fusion protein that readily crystallized in complex with Ucn1, -2, or -3. Diffraction data were collected for the three crystal forms, and the structures were solved by molecular replacement. The data collection and refinement statistics are listed in Table 1. The Ucn1-bound structure was refined to R_{work}/R_{free} values of 23.9/27.3% at 2.75 Å resolution. The Ucn2-bound structure was refined to R_{work}/R_{free} values of 22.9/26.8% at 2.72 Å, and the Ucn3-bound structure was refined to R_{work}/R_{free} values of 22.8/27.7% at 2.50 Å resolution.

The Ucn1-bound crystal form contained four fusion protein molecules (A, B, C, and D) in the asymmetric unit (ASU), each of which was bound to a Ucn1 peptide (E, F, G, and H). The Ucn2-bound crystal form also contained four fusion protein molecules in the ASU, but only molecules C and D had observable electron density for the peptide. Thus, molecules A and B are in a ligand-free state. The Ucn-3 bound crystal form contained two fusion protein molecules in the ASU, with molecule B bound to Ucn3 and molecule A in the ligand-

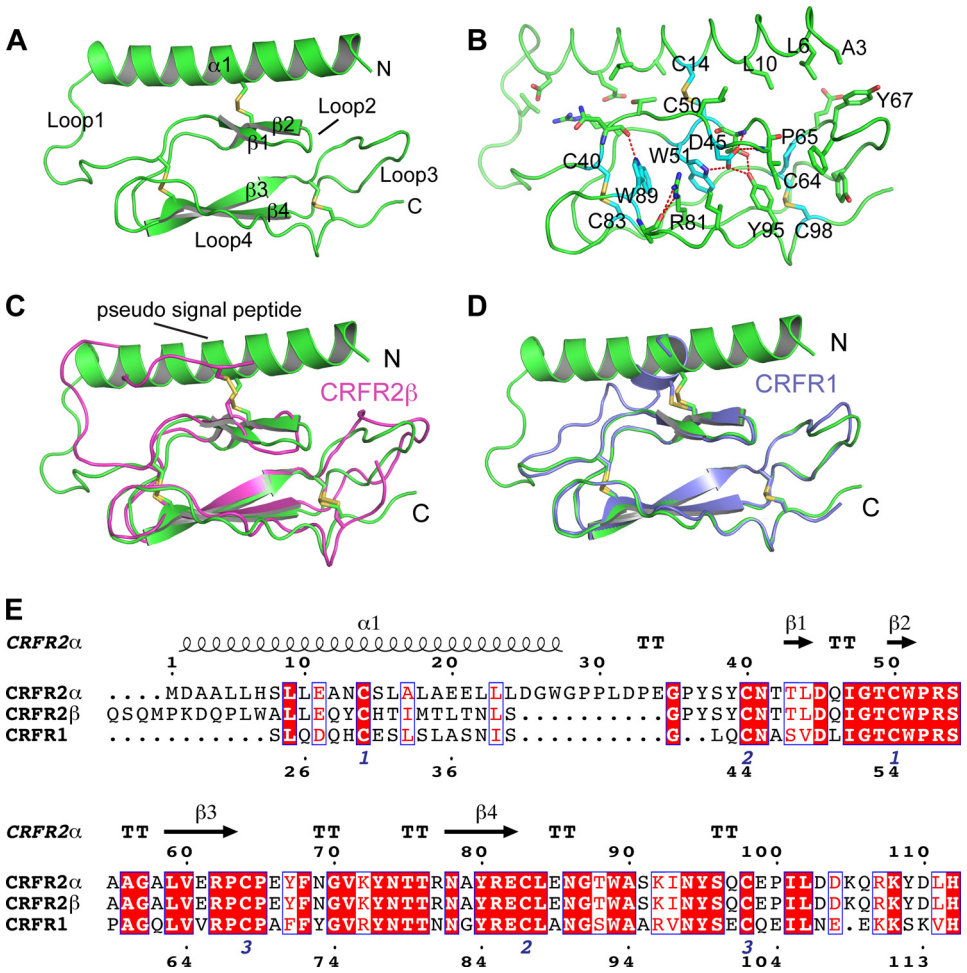

FIGURE 2. **Structure of the CRFR2α extracellular domain and comparison to CRFR2β and CRFR1.** *A*, a ribbon diagram shows the 2.5 Å resolution structure of the human CRFR2α ECD from molecule A of the Ucn3-bound crystal form. This molecule did not have a bound Ucn3 peptide and is, thus, in the ligand-free state. MBP is not shown for clarity. *B*, CRFR2α ECD shows selected side chains. The residues with carbon atoms colored *cyan* are strictly conserved among all class B GPCRs. *Red dashes* indicate hydrogen bonds. *C*, shown is a comparison of the CRFR2α ECD with the mouse CRFR2β ECD from the ligand-free NMR solution structure (PDB code 2JNC). *D*, shown is a comparison of the CRFR2α ECD with the human CRFR1 ECD from the crystal structure of CRFR1 bound to CRF (PDB code 3EHU). For clarity, the CRF peptide is not shown. *E*, amino acid sequence alignment of human CRFR2α, CRFR2β, and CRFR1 is shown. Secondary structural elements of CRFR2α are shown *above the sequence*. The *residue numbering on top* corresponds to CRFR2α, and the *numbering on the bottom* corresponds to CRFR1. The disulfide bond connectivity is indicated *below the sequences* in *blue numbering*. The signal peptide sequences of CRFR2β and CRFR1 are not shown.

free state. Supplemental Table 1 lists the ASU contents of the three crystal forms and the average B-factor values for each of the domains. In the following sections we focus our descriptions on the molecules that had the best electron density maps and the lowest B-factors.

The CRFR2α Pseudo Signal Peptide Forms an α-Helix That Is Linked to the Core Short Consensus Repeat Fold of the ECD through a Disulfide Bond—The crystal structures reveal that the CRFR2α ECD forms the expected short consensus repeat fold comprised of two β-sheets, connecting loops, and three disulfide bonds (Fig. 2*A*). ECD residues that are conserved among all class B GPCRs play the same structural roles in CRFR2α that were observed for other class B receptors (Fig. 2*B*). Interestingly, the CRFR2α pseudo signal peptide forms a long N-terminal α-helix that is linked to β2 through the C14-C50 disulfide bond. The helix makes extensive contacts with residues in the β1-β2 sheet but has no contact with loop 2 and only minor contact with loop 3 mediated by the side chains of Leu-6 and Tyr-67. This helix is absent in CRFR2β (Fig. 2*C*) and is significantly shortened in CRFR1 (Fig. 2*D*). The amino acid sequences of the α and β isoforms of human CRFR2 differ only in this N-terminal region, and CRFR1 and CRFR2 differ most substantially in this region (Fig. 2*E*). As a result of the pseudo signal peptide, CRFR2α resembles other class B GPCRs such as PTH1R, gastric inhibitory peptide receptor, and GLP1 receptor, which all contain a long N-terminal α-helix (32, 42, 43).

Structural Basis for Ucn1 Binding to the CRFR2α ECD—The structure of the CRFR2α ECD-Ucn1 complex indicates that Ucn1 forms a continuous α-helix that binds at the interface of loops 2, 3, and 4 (Fig. 3*A*), as expected based on previous structural studies of CRFR1 and mCRFR2β (23, 24). The pseudo signal peptide does not contribute to peptide recognition because it is too far away from the binding site to contact the ligand. Electron density was observed for residues 26′-41′ of Ucn1 (Fig. 3*B*) (peptide residues are denoted with a prime (′) to distinguish them from receptor residues). The density

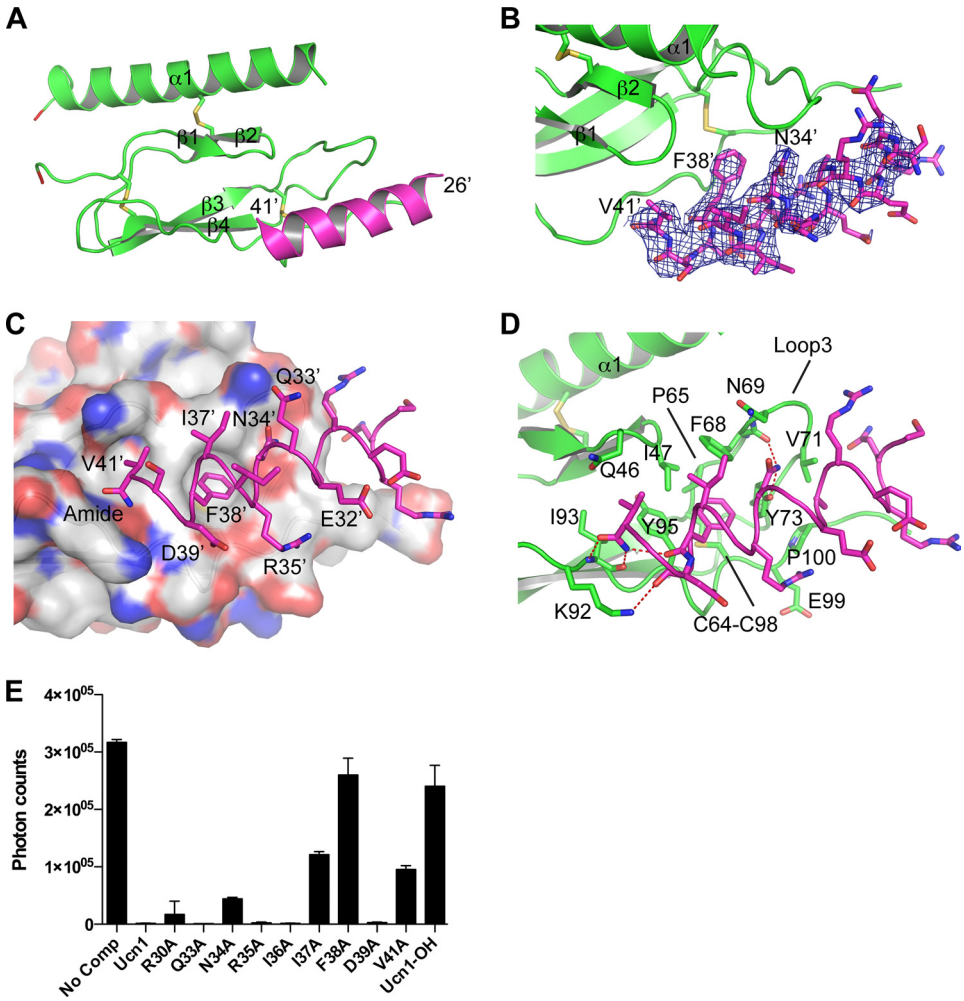

FIGURE 3. **Structure of the CRFR2α ECD-Ucn1 complex at 2.75 Å resolution.** *A*, a ribbon diagram shows the structure of the CRFR2α ECD (molecule D) in complex with Ucn1 (molecule F). The ECD is *green*, and the peptide is *magenta*. Several residues in loop 1 of the ECD were not visible in the electron density maps. The break in the chain is indicated with *red*. MBP is not shown for clarity. *B*, the $2mF_o - DF_c$ electron density map for the peptide is shown as a *blue mesh* contoured at 1 σ. *C*, a semitransparent molecular surface is shown over the ECD ribbon diagram. Carbon atoms are colored *white*, oxygen atoms are *red*, nitrogen atoms are *blue*, and sulfur atoms are *orange*. The Ucn1 peptide is shown as a *magenta coil* with selected side chains as *sticks*. *D*, shown is a detailed view of the complex with selected side chains shown as *sticks*. The *red dashes* indicate hydrogen bonds. *E*, shown is a single point competition AlphaScreen assay assessing the ability of the indicated Ucn1-(26–41) peptides (10 μM) to inhibit the association of Biotin-CRF-(12–41) and MBP-CRFR2α-(1–117)-His_6. Ucn1-OH denotes the peptide with WT amino acid sequence and a C-terminal carboxylate group instead of the amide group. The data represent the average of duplicate samples.

was better at the peptide C terminus than at the N terminus. The peptide N-terminal region exhibits higher B-factors than the C-terminal region, consistent with increased mobility of the N terminus and the C terminus serving as the "anchor point" of the interaction, as previously observed for the binding of CRF to the CRFR1 ECD (24).

The minimal pharmacophore appears to span residue Asn-34′ to the C-terminal amide group. The Asn-34′ side chain forms hydrogen bonds with the Tyr-73 side chain hydroxyl and the Phe-68 backbone carbonyl (Fig. 3*D*). The Phe-38′ phenyl ring is buried in a hydrophobic pocket of the receptor that is formed by Tyr-95, Ile-47, Pro-65, Phe-68, Tyr-73, and the Cys-64—Cys-98 disulfide (Fig. 3, *C* and *D*). Ile-37′ and Val-41′ also form hydrophobic contacts with the receptor. At the C terminus, a series of hydrogen bonds form critical contacts. The C-terminal amide nitrogen forms an intramolecular hydrogen bond with the backbone carbonyl of Phe-38′ to stabilize the helical conformation of the peptide and an intermolecular hydrogen bond with the backbone carbonyl of Ile-93 (Fig. 3*D*). In addition, the amide carbonyl group forms an intermolecular hydrogen bond with the backbone amide nitrogen of Ile-93. This pattern of hydrogen bonds was previously observed for the C-terminal amide groups of CRF and PTH interacting with their respective receptors (24, 32). Last, the electronegative peptide C terminus is capped by the positively charged Lys-92 of the receptor.

To validate the interactions observed in the crystal structure, we examined the ability of alanine-scan mutants of Ucn1 to bind to the CRFR2α ECD using the AlphaScreen assay. Alteration of residues Ile-37′, Phe-38′, or Val-41′ to alanine resulted in a peptide with diminished ability to inhibit the association of biotin-CRF and the receptor (Fig. 3*E*). In addition, substituting a carboxylate for the C-terminal amide group resulted in drastically reduced competition of the binding signal. These results indicate that the side chains of Ile-37′, Phe-38′, and Val-41′ and the C-terminal amide group are

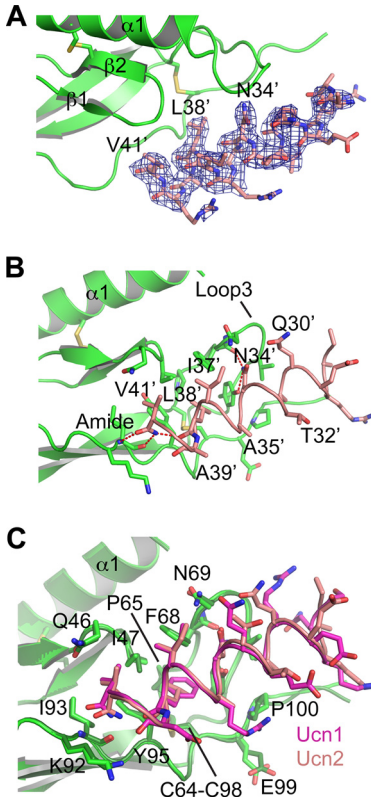

FIGURE 4. **Structure of the CRFR2α ECD-Ucn2 complex at 2.72 Å resolution.** *A*, the $2mF_o - DF_c$ electron density map for the Ucn2 peptide is shown as a *blue mesh* contoured at 1 σ. The complex shown is that of molecule D (ECD) and molecule F (Ucn2). *B*, a detailed view of the peptide-receptor interface with selected side chains is shown as *sticks*. The receptor is *green*, and the peptide is *salmon*. *C*, structural overlay of the Ucn2- and Ucn1-bound structures is shown. The ECD from the Ucn2-bound structure is *green*, and the ECD from the Ucn1-bound structure is *dark forest green*.

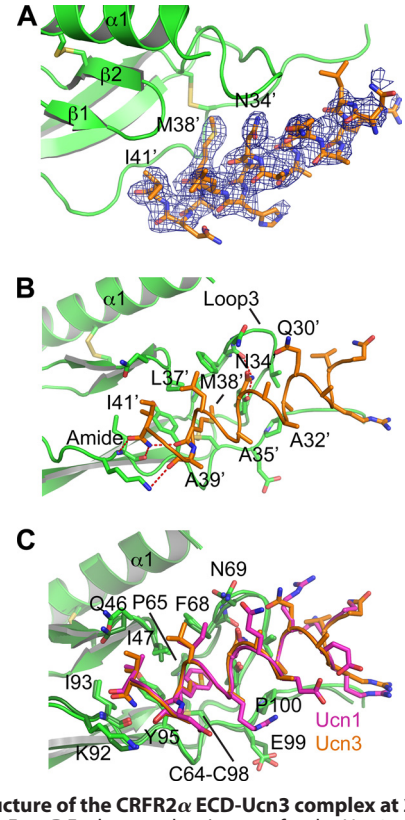

FIGURE 5. **Structure of the CRFR2α ECD-Ucn3 complex at 2.5 Å resolution.** *A*, the $2mF_o - DF_c$ electron density map for the Ucn3 peptide is shown as a *blue mesh* contoured at 1 σ. The complex shown is that of molecule B (ECD) and molecule C (Ucn3). *B*, a detailed view of the peptide-receptor interface with selected side chains is shown as *sticks*. The receptor is *green*, and the peptide is *orange*. *C*, structural overlay of the Ucn3- and Ucn1-bound structures is shown. The ECD from the Ucn3-bound structure is *green*, and the ECD from the Ucn1-bound structure is *dark forest green*.

important CRFR2α ECD binding determinants, consistent with the crystal structure.

Structural Bases for Ucn2 and Ucn3 Binding to the CRFR2α ECD—The Ucn2- and Ucn3-bound structures reveal that Ucn2 and Ucn3 bind to the CRFR2α ECD with binding modes very similar to Ucn1 despite their significantly lower affinity for the receptor. Electron density was observed for residues 26′-41′ for both Ucn2 (Fig. 4*A*) and Ucn3 (Fig. 5*A*). Residue Asn-34′ and the C-terminal amide groups of Ucn2 and Ucn3 form the same network of hydrogen bonds observed for Ucn1 (Figs. 4*B* and 5*B*). Ucn2 and Ucn3 both contain a hydrophobic residue at position 38′ (Leu in Ucn2, Met in Ucn3) that occupies the hydrophobic pocket in the receptor surface, similar to Phe-38′ of Ucn1 (Figs. 4, *B* and *C*, and 5, *B* and *C*). The most significant differences between Ucn2/3 and Ucn1 are at residues Ala-35′ and Ala-39′ in Ucn2/3, which are Arg-35′ and Asp-39′ in Ucn1 (Figs. 4*C* and 5*C*).

The Ligand-free and Ligand-bound Conformations of the CRFR2α ECD Do Not Differ Substantially—Our previous crystal structures of the ligand-free and CRF-bound states of the human CRFR1 ECD indicated that loops 2 and 4 undergo clamp-like conformational changes upon CRF binding that probably help anchor the peptide C terminus (24) (Fig. 6*A*). Similarly, NMR studies of the mouse CRFR2β ECD revealed that loops 2 and 4 exhibit conformational flexibility in the absence of ligand and become ordered upon peptide binding (23). We examined if similar changes occur in the human CRFR2α ECD by comparing the two ECD molecules that were present in the ASU of the Ucn3 crystal form; molecule A was in the ligand-free state, whereas molecule B was bound to Ucn3. In contrast to the observations for hCRFR1 and mCRFR2β, there were no substantial conformational differences between the ligand-free and Ucn-3-bound states of the hCRFR2α ECD (Fig. 6*B*). This difference appears to be determined by the presence of an Ile residue at position 93 in hCRFR2α instead of the Val residue present at the equivalent positions in hCRFR1 (Val-97) and mCRFR2β. The additional methyl group contributed by Ile-93 in hCRFR2α would clash with the side chain of the conserved Asp residue in loop 2 (Asp-45 in hCRFR2α) if similar clamp-like motions occurred (Fig. 6, *A* and *B*).

Structural Basis for Ligand Selectivity—Structural elements that determine the selectivity of Ucn2/3 for CRFR2 were examined by comparing the CRFR2α ECD-Ucn3 structure with our previous structure of the CRFR1 ECD-CRF complex (24). The Ucn3-bound structure was chosen for comparison because Ucn3 shares more sequence identity with CRF than Ucn2 (Fig. 1*A*), and the Ucn3 structure was determined to a higher resolution. Structural overlay of the two complexes reveals that the peptides bind to their respective receptors with nearly identical binding modes (Fig. 7*A*). CRF and Ucn3

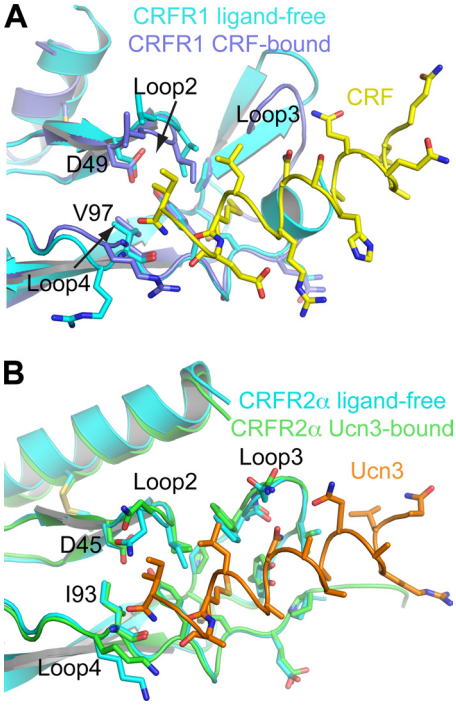

FIGURE 6. **Comparison of the ligand-free and ligand-bound states of CRFR1 and CRFR2α.** *A*, shown is structural overlay of the ligand-free (2.75 Å resolution; PDB code 3EHS) and CRF-bound (1.96 Å resolution; PDB code 3EHU) structures of the CRFR1 ECD. The *arrows* indicate the direction of the shifts observed for loop 2 and loop 4 upon CRF binding. Differences in loop 3 cannot be attributed to ligand effects because a crystal packing interaction in the ligand-free structure caused loop 3 to form a presumably unnatural conformation. *B*, structural overlay of the ligand-free (molecule A) and Ucn3-bound (molecules B and C) structures of the CRFR2α ECD is shown.

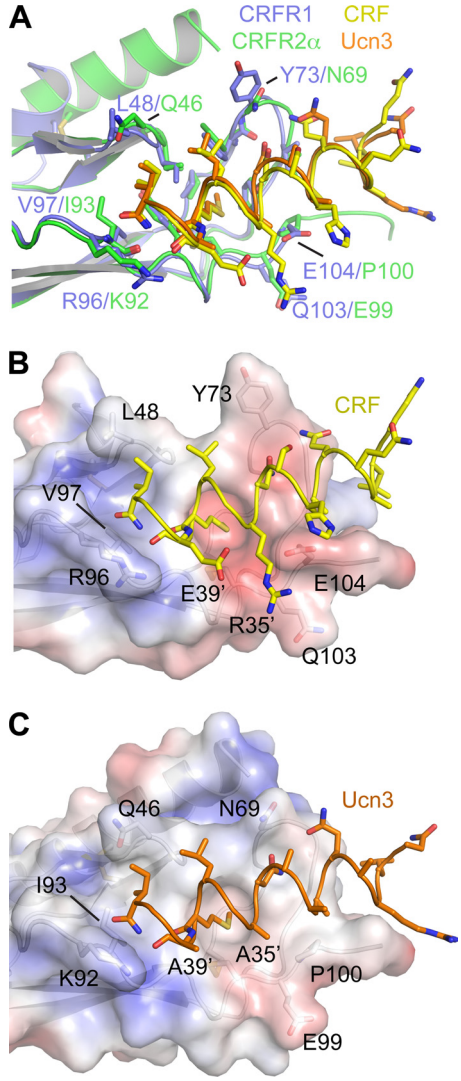

FIGURE 7. **Comparison of the CRFR2α ECD-Ucn3 and CRFR1 ECD-CRF complexes.** *A*, structural overlay of the CRFR2α ECD-Ucn3 complex (2.5 Å resolution) with the CRFR1 ECD-CRF complex (1.9 Å resolution; PDB code 3EHU) is shown. The CRFR2α ECD-Ucn3 complex is that of molecules B and C, respectively. The ECDs are shown as *ribbon diagrams* with side chains that form the peptide-binding site shown as *sticks*. The peptides are shown as coils with selected side chains as *sticks*. The six peptide-binding site residues that differ between CRFR1 and CRFR2α are labeled in color-coded format. CRFR1 residue Tyr-73 exhibited no side chain electron density in the 3EHU structure and was, thus, trimmed back to the β carbon atom in 3EHU. For clarity, here the Tyr-73 side chain was added in the most sensible rotamer conformation. *B*, the electrostatic surface potential of the CRFR1 ECD was calculated with APBS assuming a solvent of 150 mM salt. A semitransparent molecular surface colored according to charge is shown *over the CRFR1 ribbon diagram*. The color ramp is from −5 (*red*) to +5 (*blue*) *kT/e*. The side chains of the six peptide-binding site residues that differ between CRFR1 and CRFR2α are shown as *sticks* and labeled. CRF is shown as a *yellow coil*. To permit better comparison with CRFR2α, residues 105–106 of CRFR1, which were not visible in the electron density maps for 3EHU, were added to the ECD in the same conformation observed for residues 101–102 of CRFR2α. These residues are strictly conserved between CRFR1 and CRFR2α (Fig. 2*E*). *C*, shown is the electrostatic surface potential of the CRFR2α ECD, depicted as in *panel B*. Ucn3 is shown as an *orange coil*.

share Asn-34′, Leu-37′, Met-38′, and Ile-41′, which form identical contacts in the two structures. The architectures of the peptide-binding sites are very similar, with only six residues located at the periphery of the binding sites differing between CRFR1 and CRFR2α (Figs. 7*A* and 2*E*).

Comparing the electrostatic surface potentials of the two receptor ECDs suggests that the single CRFR1 Glu-104/CRFR2α Pro-100 difference determines the selectivity profiles of the receptors by a charge compatibility mechanism. Residue Glu-104 creates a negative area of the CRFR1 receptor surface adjacent to peptide residue 35′ (Fig. 7*B*). The positively charged Arg-35′ of CRF/Ucn1 is electrostatically compatible with Glu-104, whereas the hydrophobic Ala-35′ of Ucn2/3 would serve as a repelling force. In contrast, residue Pro-100 creates a hydrophobic surface on the CRFR2α receptor adjacent to peptide residue 35′ (Fig. 7*C*) that would be compatible with the nonpolar Ala-35′ of Ucn2/3 as well as the aliphatic portion of the Arg-35′ side chain of CRF/Ucn1. Thus, we propose that CRFR1 residue Glu-104 is the "selectivity filter" that prevents Ucn2/3 binding.

Functional Basis for Ligand Selectivity—In a previous study, Mazur *et al.* (28) assessed the ability of full-length CRF/Ucn peptides altered at positions 35′ and 39′ to stimulate cAMP accumulation in cells expressing either CRFR1 or CRFR2 and demonstrated that alanine at positions 35′ and 39′ contributed to CRFR2 selectivity (28). Our crystal structures provide a molecular rationale for why position 35′ and, to a lesser extent position 39′, determine receptor selectivity. To further examine positions 35′ and 39′, we assessed the CRFR1 and CRFR2α ECD binding ability of hybrid Ucn1/3 peptides containing reciprocal swap mutations at positions 35′ and 39′. The single R35′A mutation was sufficient to drastically reduce the binding of Ucn1 to CRFR1 (Fig. 8*A*) and also decreased its

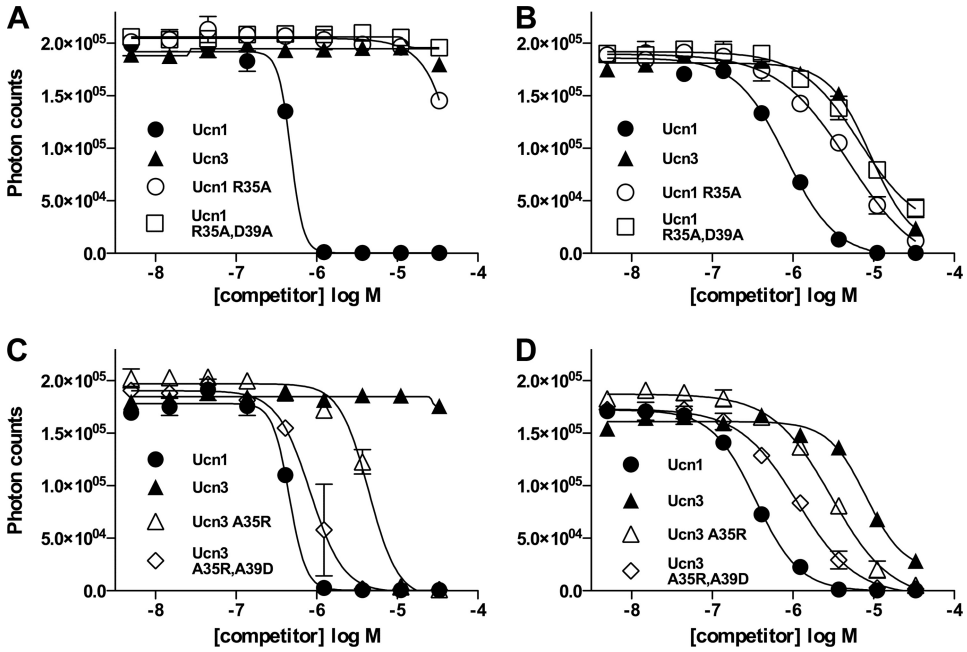

FIGURE 8. **Binding of Ucn1/3 swap peptides to the CRFR1 and CRFR2α ECDs.** Competition binding curves show the ability of the indicated peptides to inhibit the association of biotin-CRF-(12–41) and the MBP-CRFR1.24–119-His_6 (*A* and *C*) or MBP-CRFR2α-(1–117)-His_6 (*B* and *D*) fusion proteins in the AlphaScreen assay. The data represent the average of duplicate samples.

affinity for CRFR2α (Fig. 8*B*). The R35′A/D39′A Ucn1 double mutant did not exhibit detectable CRFR1 binding and bound to CRFR2α with an affinity comparable with Ucn3 (Fig. 8, *A* and *B*). Similarly, the single A35′R mutation was able to impart CRFR1 binding ability to Ucn3 (Fig. 8*C*) and slightly increase its affinity for CRFR2α (Fig. 8*D*). Inclusion of the A39′D mutation in combination with A35′R further increased the affinity of Ucn3 for both receptors, although not to the level of WT Ucn1 (Fig. 8, *C* and *D*). These results indicate that the residues at peptide positions 35′ and, to a lesser extent 39′, are sufficient to determine receptor specificity via effects on ECD binding, and they complement the results reported for the full-length receptor (28). Together these results support the proposed electrostatic compatibility mechanism mediated by the CRFR1 residue Glu-104 selectivity filter.

DISCUSSION

The CRF/Ucn family of peptides and their two receptors constitute an important biological system that controls central stress/anxiety responses, links stress and metabolic energy homeostasis, and regulates cardiovascular, immune, gastrointestinal, and reproductive functions. The three crystal structures presented here show for the first time how the Ucn peptides are recognized by the CRFR2 receptor and reveal the structural basis for ligand discrimination by the CRFR1 and CRFR2 ECDs. Peptide binding assays demonstrated that the isolated ECDs of CRFR1 and CRFR2 are sufficient to discriminate the peptides with the same rank order as the full-length receptors, indicating that the ECDs act as selectivity filters that determine ligand specificity in addition to their role in enabling high affinity ligand binding. Thus, it appears that the ECDs provide an important "filtering" step in the ligand binding process, although the 7-transmembrane domains can also contribute to ligand selectivity through interactions with the N-terminal region of the peptides (25, 28).

The CRFR2α ECD formed the same fold previously observed for the hCRFR1 and mCRFR2β ECDs with the exception of the long N-terminal α-helix formed by the pseudo signal peptide. This helix renders the CRFR2α ECD similar in appearance to those of other class B GPCRs, such as PTH1R, gastric inhibitory peptide receptor, and GLP1 receptor, which also contain a long N-terminal helix (32, 42, 43). In these other receptors, the N-terminal helix forms part of the peptide-binding site. In contrast, the CRFR2α ECD helix does not affect ligand binding because the ECD peptide-binding site in the CRF receptors is significantly shifted away from the N-terminal helix as compared with other class B GPCRs (24). If the pseudo signal peptide were cleaved from CRFR2α, Cys-50 would be left unpaired, but the peptide-binding site would remain intact. Indeed, before it was understood that CRFR2α contains a pseudo signal peptide, Klose *et al.* (44) demonstrated that a recombinant form of the rat CRFR2α ECD that lacked the presumed signal peptide contained an unpaired Cys-50 residue and retained the ability to bind Ucn1. Interestingly, the γ isoform of CRFR2 would have five cysteine residues if the putative signal peptide were cleaved and six if it were not removed. Thus, CRFR2γ may also have a pseudo signal peptide that is linked to the core short consensus repeat fold of the ECD through a disulfide bond.

The CRFR2α ECD peptide-binding site architecture is very similar to that of CRFR1, with only six residues at the periphery of the binding sites differing between the receptors (Fig. 7). This result was not completely expected because the NMR structure of the mCRFR2β ECD in complex with astressin (23) indicated a very different loop 3 conformation than was observed for the CRFR1 ECD (24). The structures reported

here clearly indicate that the CRFR2 ECD loop 3 conformation is in fact quite similar to CRFR1. The binding of the Ucn peptides to the CRFR2α ECD closely resembles the binding of CRF to the CRFR1 ECD. Comparing the electrostatic surface potentials of the two ECDs suggested that Glu-104 of CRFR1, which is replaced by Pro-100 in CRFR2α, acts as a selectivity filter preventing the binding of Ucn2/3 by a charge compatibility mechanism. Ucn2 and -3 contain the nonpolar residue Ala-35′ instead of the positively charged Arg-35′ present in CRF/Ucn1. The uncharged, hydrophobic Ala-35′ presumably provides a repelling force to the negatively charged Glu-104, whereas the positively charged Arg-35′ of CRF/Ucn1 provides an attractive force. Presumably, Arg-35′ does not prevent CRFR2 binding because the aliphatic portion of the side chain is compatible with Pro-100. We previously proposed such a mechanism based on our structure of the CRFR1 ECD-CRF complex and peptide binding data that showed that the Arg-35′ side chain of CRF was absolutely required for CRFR1 ECD binding even though the electron density maps for our structure (PDB code 3EHU) did not provide evidence for an intermolecular salt bridge between CRF Arg-35′ and CRFR1 Glu-104 (24). The recently reported NMR solution structure of the hCRFR1 ECD bound to a high affinity CRF-like agonist showed that Arg-35′ of the peptide is in proximity to Glu-104 of the receptor (31).

In support of our proposed selectivity mechanism, our ECD binding data for the hybrid Ucn1/3 swap peptides (Fig. 8) confirmed the importance of peptide residue 35′ for determining selectivity. However, the data also indicated that peptide residue 39′ cooperates with residue 35′ to contribute to selectivity and affinity, especially in the context of converting Ucn3 into a non-selective peptide. This point is highlighted by our data showing that the Ucn3 A35′R/A39′D double mutant exhibited higher affinity for both ECDs than the A35′R single mutant (Fig. 8, *C* and *D*). One possible explanation is that an intramolecular salt bridge between Arg-35′ and Asp-39′ stabilizes the helical conformation of the peptide and, thus, increases its affinity. In the case of CRFR1 binding, a competition between Asp-39′ of the peptide and Glu-104 of CRFR1 for the Arg-35′ side chain might exist. For binding to CRFR2, the formation of an intramolecular Arg-35′–Asp-39′ salt bridge would presumably facilitate the exposure of the aliphatic portion of the Arg-35′ side chain to Pro-100. The electron density maps for the Ucn1-CRFR2α ECD structure were not well defined for the side chains of Arg-35′ and Asp-39′, similar to our CRF-CRFR1 ECD structure lacking side chain density for CRF Arg-35′ and Glu-39′; thus, we do not have crystallographic evidence supporting Ucn1 Arg-35′-Asp-39′ interactions. Nonetheless, the peptide binding data clearly support a role for functional coupling between peptide residues 35′ and 39′. Moreover, our results are entirely consistent with those reported in the literature for the full-length peptides acting at intact receptors in cells. Mazur *et al.* (28) demonstrated that substituting alanine at positions 35′ and 39′ of Ucn1 contributed to significantly reduced potency at CRFR1 while having little effect on potency at CRFR2, further supporting the charge compatibility mechanism for ligand selectivity as observed from our ECD structures.

The structures reported here provide us with more complete views of the mechanisms of ligand recognition used by the CRF receptors and increase our understanding of the molecular basis for peptide selectivity. From a translational standpoint, the structures provide additional templates to guide rational drug design efforts. The similarity of the CRFR1 and CRFR2 ECD peptide-binding site architectures highlights the challenges associated with developing drugs that selectively target one receptor ECD over the other. Fortunately, the distinct electrostatic surface potentials arising from the CRFR1 Glu-104/CRFR2α Pro-100 difference provides a possible route to developing drugs that selectively target the ECDs. The fact that the endogenous ligands Ucn2/3 can selectively target CRFR2 based on this charge difference bodes well for our ability to exploit this mechanism for therapeutic purposes.

Acknowledgments—We thank J. Brunzelle for assistance with data collection at sector 21 (LS-CAT) of the Advanced Photon Source, which is partly funded by the Michigan Economic Development Corp. and Michigan Technology Tri-Corridor Grant 085P1000817. Use of the Advanced Photon Source was supported by the Office of Science of the United States Department of Energy.

REFERENCES

1. Bale, T. L., and Vale, W. W. (2004) *Annu. Rev. Pharmacol. Toxicol.* **44,** 525–557
2. Hauger, R. L., Risbrough, V., Brauns, O., and Dautzenberg, F. M. (2006) *CNS Neurol. Disord Drug Targets* **5,** 453–479
3. Hillhouse, E. W., and Grammatopoulos, D. K. (2006) *Endocr. Rev.* **27,** 260–286
4. Chen, R., Lewis, K. A., Perrin, M. H., and Vale, W. W. (1993) *Proc. Natl. Acad. Sci. U.S.A.* **90,** 8967–8971
5. Hsu, S. Y., and Hsueh, A. J. (2001) *Nat. Med.* **7,** 605–611
6. Lewis, K., Li, C., Perrin, M. H., Blount, A., Kunitake, K., Donaldson, C., Vaughan, J., Reyes, T. M., Gulyas, J., Fischer, W., Bilezikjian, L., Rivier, J., Sawchenko, P. E., and Vale, W. W. (2001) *Proc. Natl. Acad. Sci. U.S.A.* **98,** 7570–7575
7. Perrin, M., Donaldson, C., Chen, R., Blount, A., Berggren, T., Bilezikjian, L., Sawchenko, P., and Vale, W. (1995) *Proc. Natl. Acad. Sci. U.S.A.* **92,** 2969–2973
8. Reyes, T. M., Lewis, K., Perrin, M. H., Kunitake, K. S., Vaughan, J., Arias, C. A., Hogenesch, J. B., Gulyas, J., Rivier, J., Vale, W. W., and Sawchenko, P. E. (2001) *Proc. Natl. Acad. Sci. U.S.A.* **98,** 2843–2848
9. Vaughan, J., Donaldson, C., Bittencourt, J., Perrin, M. H., Lewis, K., Sutton, S., Chan, R., Turnbull, A. V., Lovejoy, D., Rivier, C., *et al.* (1995) *Nature* **378,** 287–292
10. Grace, C. R., Perrin, M. H., Cantle, J. P., Vale, W. W., Rivier, J. E., and Riek, R. (2007) *J. Am. Chem. Soc.* **129,** 16102–16114
11. Fekete, E. M., and Zorrilla, E. P. (2007) *Front. Neuroendocrinol.* **28,** 1–27
12. Chen, A., Brar, B., Choi, C. S., Rousso, D., Vaughan, J., Kuperman, Y., Kim, S. N., Donaldson, C., Smith, S. M., Jamieson, P., Li, C., Nagy, T. R., Shulman, G. I., Lee, K. F., and Vale, W. (2006) *Proc. Natl. Acad. Sci. U.S.A.* **103,** 16580–16585
13. Kuperman, Y., Issler, O., Regev, L., Musseri, I., Navon, I., Neufeld-Cohen, A., Gil, S., and Chen, A. (2010) *Proc. Natl. Acad. Sci. U.S.A.* **107,** 8393–8398
14. Li, C., Chen, P., Vaughan, J., Lee, K. F., and Vale, W. (2007) *Proc. Natl. Acad. Sci. U.S.A.* **104,** 4206–4211
15. Kuperman, Y., and Chen, A. (2008) *Trends Endocrinol. Metab.* **19,** 122–129
16. Bale, T. L., Giordano, F. J., and Vale, W. W. (2003) *Trends Cardiovasc. Med.* **13,** 68–71

17. Hao, Z., Huang, Y., Cleman, J., Jovin, I. S., Vale, W. W., Bale, T. L., and Giordano, F. J. (2008) *Proc. Natl. Acad. Sci. U.S.A.* **105,** 3939–3944
18. Wang, J., Xu, Y., Xu, Y., Zhu, H., Zhang, R., Zhang, G., and Li, S. (2008) *Cancer Invest* **26,** 359–368
19. Grammatopoulos, D. K., and Chrousos, G. P. (2002) *Trends Endocrinol Metab.* **13,** 436–444
20. Yang, L. Z., Tovote, P., Rayner, M., Kockskämper, J., Pieske, B., and Spiess, J. (2010) *Eur. J. Pharmacol.* **632,** 1–6
21. Dieterle, T., Meili-Butz, S., Bühler, K., Morandi, C., John, D., Buser, P. T., Rivier, J., Vale, W. W., Peterson, K. L., and Brink, M. (2009) *Hypertension* **53,** 739–744
22. Hoare, S. R. (2005) *Drug Discov. Today* **10,** 417–427
23. Grace, C. R., Perrin, M. H., Gulyas, J., Digruccio, M. R., Cantle, J. P., Rivier, J. E., Vale, W. W., and Riek, R. (2007) *Proc. Natl. Acad. Sci. U.S.A.* **104,** 4858–4863
24. Pioszak, A. A., Parker, N. R., Suino-Powell, K., and Xu, H. E. (2008) *J. Biol. Chem.* **283,** 32900–32912
25. Dautzenberg, F. M., Kilpatrick, G. J., Wille, S., and Hauger, R. L. (1999) *J. Neurochem.* **73,** 821–829
26. Perrin, M. H., DiGruccio, M. R., Koerber, S. C., Rivier, J. E., Kunitake, K. S., Bain, D. L., Fischer, W. H., and Vale, W. W. (2003) *J. Biol. Chem.* **278,** 15595–15600
27. Perrin, M. H., Fischer, W. H., Kunitake, K. S., Craig, A. G., Koerber, S. C., Cervini, L. A., Rivier, J. E., Groppe, J. C., Greenwald, J., Møller Nielsen, S., and Vale, W. W. (2001) *J. Biol. Chem.* **276,** 31528–31534
28. Mazur, A. W., Wang, F., Tscheiner, M., Tcheiner, M., Donnelly, E., and Isfort, R. J. (2004) *J. Med. Chem.* **47,** 3450–3454
29. Zmijewski, M. A., and Slominski, A. T. (2010) *Acta Biochim. Pol.* **57,** 1–13
30. Rutz, C., Renner, A., Alken, M., Schulz, K., Beyermann, M., Wiesner, B., Rosenthal, W., and Schülein, R. (2006) *J. Biol. Chem.* **281,** 24910–24921
31. Grace, C. R., Perrin, M. H., Gulyas, J., Rivier, J. E., Vale, W. W., and Riek, R. (2010) *J. Biol. Chem.* **285,** 38580–38589
32. Pioszak, A. A., and Xu, H. E. (2008) *Proc. Natl. Acad. Sci. U.S.A.* **105,** 5034–5039
33. Otwinowski, Z., and Minor, W. (1997) *Methods Enzymol.* **276,** 307–326
34. McCoy, A. J., Grosse-Kunstleve, R. W., Adams, P. D., Winn, M. D., Storoni, L. C., and Read, R. J. (2007) *J. Appl. Crystallogr.* **40,** 658–674
35. Collaborative Computational Project, N. (1994) *Acta Crystallogr. D. Biol. Crystallogr.* **50,** 760–763
36. Emsley, P., and Cowtan, K. (2004) *Acta Crystallogr. D. Biol. Crystallogr.* **60,** 2126–2132
37. Murshudov, G. N., Vagin, A. A., and Dodson, E. J. (1997) *Acta Crystallogr. D. Biol. Crystallogr.* **53,** 240–255
38. Pioszak, A. A., Parker, N. R., Gardella, T. J., and Xu, H. E. (2009) *J. Biol. Chem.* **284,** 28382–28391
39. DeLano, W. L. (2002) *The PyMOL Molecular Graphics System*, DeLano Scientific LLC, San Carlos, CA
40. Baker, N. A., Sept, D., Joseph, S., Holst, M. J., and McCammon, J. A. (2001) *Proc. Natl. Acad. Sci. U.S.A.* **98,** 10037–10041
41. Pioszak, A. A., Harikumar, K. G., Parker, N. R., Miller, L. J., and Xu, H. E. (2010) *J. Biol. Chem.* **285,** 12435–12444
42. Parthier, C., Kleinschmidt, M., Neumann, P., Rudolph, R., Manhart, S., Schlenzig, D., Fanghänel, J., Rahfeld, J. U., Demuth, H. U., and Stubbs, M. T. (2007) *Proc. Natl. Acad. Sci. U.S.A.* **104,** 13942–13947
43. Runge, S., Thøgersen, H., Madsen, K., Lau, J., and Rudolph, R. (2008) *J. Biol. Chem.* **283,** 11340–11347
44. Klose, J., Fechner, K., Beyermann, M., Krause, E., Wendt, N., Bienert, M., Rudolph, R., and Rothemund, S. (2005) *Biochemistry* **44,** 1614–1623